Journal of Hazardous Materials 411 (2021) 124971

Contents lists available at ScienceDirect

Journal of Hazardous Materials

journal homepage: www.elsevier.com/locate/jhazmat

Research paper

Downregulation of the photosynthetic machinery and carbon storage signaling pathways mediate La_2O_3 nanoparticle toxicity on radish taproot formation

Zhenggao Xiao [a], Le Yue [a], Chuanxi Wang [a], Feiran Chen [a], Ying Ding [a], Yinglin Liu [a], Xuesong Cao [a], Zhe Chen [b], Sergio Rasmann [c], Zhenyu Wang [a,*]

[a] Institute of Environmental Processes and Pollution Control, and School of Environmental and Civil Engineering, Jiangnan University, Wuxi 214122, China
[b] Institute of Tropical Fruit Trees, Hainan Academy of Agricultural Science, Haikou 571100, China
[c] Institute of Biology, University of Neuchâtel, Rue-Emile-Argand 11, 2000 Neuchâtel, Switzerland

ARTICLE INFO

Editor: Dr. S Nan

Keywords:
Lanthanum oxide nanoparticles
Nanotoxicity
Cell wall composition
Root cracking
Transcriptome

ABSTRACT

The molecular and physiological mechanisms of how rare earth oxide nanoparticles (NPs) alter radish (*Raphanus sativus* L.) taproot formation and cracking were investigated in the present study. We compared plants that received suspensions of 10, 50, 100, 300 mg L^{-1} of La_2O_3 NPs, 300 m L^{-1} La_2O_3 bulk-particles (BPs), 0.8 m L^{-1} La^{3+}, or only water for six days during their tuber formation period. 100 and 300 mg L^{-1} La_2O_3 NPs exposure decreased storage root biomass by 38% and 60%, respectively, and they both induced visible root cracking. Physiological analyses showed that La_2O_3 NPs exposure (>100 mg L^{-1}) significantly inhibited leaf net photosynthetic rate, cell wall pectin synthesis of both storage root epidermis and xylem parenchyma tissues, but increased the contents of cellulose and hemicellulose 1 in root epidermis cell walls. Moreover, transcriptome analysis further found that La_2O_3 NPs changed root cell wall structure by down-regulating core genes involved in cell wall pectin and IAA biosynthesis, which coincided with the observed La_2O_3 NPs-induced root cracking. Our results revealed the molecular mechanisms related to cell wall carbohydrate metabolism in response to NPs stress, providing a step forward for understanding the causes of NPs phytotoxicity on edible plant taproot formation and cracking.

1. Introduction

Rare earth oxide nanoparticles (ROE NPs) are commonly used in high-technology industries and biomedical fields because of their magnetic, catalytic, and optic properties (Ma et al., 2010; Hwang et al., 2019). Lanthanum oxide nanoparticles (La_2O_3 NPs) are among the most widespread ROE NPs, as they can be used for building electric sensors, catalysts, paint coatings, polishing powders, fuel cells, antimicrobials, or water treatment devices (Balusamy et al., 2012; Sisler et al., 2016; Lu and McDonald, 2020). Due to their widespread daily usage, La_2O_3 NPs have inevitably been released into the natural environment, leading to adverse effects on plant physiological processes and crop productivity (De la Torre Roche et al., 2015; Rizwan et al., 2017; Hwang et al., 2019). Hence, the evaluation of the effects of La_2O_3 NPs on the crop plant-edible parts, as well as on the general food safety, has received increasing attention (Hwang et al., 2019).

Several studies have shown that La_2O_3 NPs can accumulate in the roots and shoots of plant, but the effect of La_2O_3 NPs on plant physiological and biochemical parameters varies depending on different plant types, exposure dose and growing conditions (hydroponic or soil culture). For instance, La_2O_3 NP suspensions at around 2 mg L^{-1} were sufficient to inhibit the accumulation of root and shoot biomass in cucumber (*Cucumis sativus*) plants, while 2000 mg L^{-1} of La_2O_3 NPs were needed to induce more reactive oxygen species and cell death in *C. sativus* roots (Ma et al., 2015). Similarly, under hydroponic conditions, a minimum of 500 mg L^{-1} of La_2O_3 NPs was needed to significantly decrease root and shoot biomass of maize (*Zea mays*) plants (Yue et al., 2017), 2000 mg L^{-1} La_2O_3 NPs resulted in reduced root elongation of radish (*R. sativus*) seedlings (Ma et al., 2010), even 10 mg L^{-1} La_2O_3 NP suspension reduced the net photosynthetic rate of soybean and maize by 8.77% and 55.52%, respectively (Liu et al., 2020). A recent study also showed that the inhibitory effects of La_2O_3 NPs on maize growth were

* Corresponding author.
E-mail address: wang0628@jiangnan.edu.cn (Z. Wang).

https://doi.org/10.1016/j.jhazmat.2020.124971
Received 20 October 2020; Received in revised form 18 December 2020; Accepted 23 December 2020
Available online 25 December 2020

related to the up-regulation of core genes involved in lignin synthesis, since the lignin-enriched apoplastic barriers in juvenile maize led to the reduction of stomatal conductance and transpiration rate (Yue et al., 2019). Moreover, 500 mg kg^{-1} of La_2O_3 NPs soil exposure reduced lettuce shoot biomass by 23–30% (De la Torre Roche et al., 2015). Although the phytoxicity of La_2O_3 NPs some plant growth and physiological parameter has been documented, little is yet known about the effects of La_2O_3 NPs on the growth and development of edible plant roots, a matter that is are directly related to food safety (Rizwan et al., 2017; Hwang et al. 2019).

Since the edible parts of root crops are developed in the soil, or immersed the hydroponic solution, it is very likely to have direct contact to La_2O_3 NPs, and the potential negative effects of La_2O_3 NPs accumulation in food crops could be expected. Specifically for radish, healthy edible taproots have a crisp and crunchy texture, while under stress, root cracking occurs easily, ultimately resulting in severely decrease in yield and commercial value of radishes (Yu et al., 2019). Taproot thickening is a process characterized by the formation of secondary cell walls, which are richer in microfibrils and lignin than that of the primary cell walls of younger roots, which in turn are richer in carbohydrates (Somerville et al., 2004; Yu et al., 2016). When faced with environmental stress, the mechanical properties of cell walls (e.g., viscosity and elasticity) can be altered via changes in the composition and structure of cell walls (Sun et al., 2016). For instance, it has been found that Fe^0 NPs exposure slightly decreased the carbohydrate and lignin contents of alfalfa root cell wall (Kim et al., 2019), and CuO NPs decreased the cell wall xyloglucan and esterified pectin contents in the roots of *Arabidopsis thaliana* seedlings (Nie et al., 2020). To date, however, the genetic and physiological changes in the cell wall synthesis of the radish storage root epidermis and xylem parenchyma tissues in response to NPs stress have not been characterized. Therefore, by clarifying the molecular mechanism underlying the processes mediating radish storage root development and cracking in response to La_2O_3 NPs will be potentially possible to breed more radish varieties resistant to root cracking in the future (Yu et al., 2019).

In the present study, we addressed the phytotoxicity of La_2O_3 NPs on radish plants by measuring growth performance, root cell wall composition, photosynthetic parameters and La uptake and distribution of radish tissues during taproot expansion in a soilless hydroponic culture system. Moreover, we clarified the underlying molecular mechanism of root cracking in response to La_2O_3 NPs exposure using transcriptome analyses. Finally, we validated the expression of the candidate genes involved in the biosynthesis pathways of cell wall carbohydrates and phytohormones for regulating cell enlargement/division. The following three questions were addressed: 1) Is the effect of La_2O_3 NPs on radish reproductive growth dose-dependent? 2) Do La_2O_3 NPs change cell wall composition of radish root epidermis and xylem parenchyma tissues? 3) What are the underlying molecular mechanisms of La_2O_3 NPs-induced radish storage root cracking? We predicted 1) a positive dose-dependent La_2O_3 NPs-phytotoxicity relationship, 2) a significant fragilization of in the radish root tissues due to the significant structural molecular changes after La_2O_3 NPs exposure, and 3) a downregulation of key genes related to cell wall thickening when radish roots are exposed to La_2O_3 NPs. This is the first evidence of the molecular and physiological mechanisms addressing the detrimental effects of La_2O_3 nanoparticles on radish edible root formation and root cracking. These findings would provide important information to support the safe and sustainable application of nanomaterials in agriculture.

2. Materials and methods

2.1. La_2O_3 NPs preparation and characterization

La_2O_3 NPs (99.9%, 10–100 nm) and bulk-particles (BPs) (99.9%) were purchased from US Research Nanomaterials (Houston, TX, USA) and Sinopharm Chemical Reagent Co., Ltd (Shanghai, China), respectively. Aqueous suspensions of both La_2O_3 NPs and La_2O_3 BPs were prepared via adding their respective powders to deionized water and subsequently sonicated (100 W, 40 kHz, 30 ℃) the mixture for 30 min to increase dispersion. The morphology of the La_2O_3 NPs and La_2O_3 BPs was observed using transmission electron microscopy (TEM, JEM-2100, Japan) operated at 200 kV. The TEM images indicated that the sizes of the La_2O_3 NPs and La_2O_3 BPs were in average 58 nm and 0.65 μm, respectively (Fig. S1). To characterize the suspension stability and dissolution behavior of NPs in the aqueous environment, the hydrodynamic particle size and ζ-potential of La_2O_3 NPs in the presence or absence of radish plants for 48 h were measured with a Malvern NanoZS analyzer (Malvern Instrument Inc., UK) (Table S1). The time-dependent dissolution of La_2O_3 NPs in deionized water with or without presence of plants was determined at 24 h and 48 h using triple quadrupole inductively coupled plasma mass spectrometry (ICP-MS) (Thermo Fisher, Germany). In order to evaluate the precision and accuracy of the methods, a standard reference material (bush branches and leaves, GBW07602) and spiked sample (spiked with stock standard solution at 1 mg Kg^{-1} of La) were also analyzed by the same procedure. Germanium (10 μg mL^{-1}) was used as an internal standard to calibrate the instrument signal drift and matrix suppression. The calibration curve for La element was obtained by standard addition method, and linearity range and equation, detection limit, spike recovery were shown in Table S2. For quality control (QC), the La elemental standard solution was evaluated every 10 samples.

2.2. Plant cultivation and La_2O_3 NP exposure

Radish (*Raphanus sativus* L.) plants are cultivated and consumed worldwide due to their abundant nutritive and antioxidant properties (e.g. carbohydrates, crude fiber, vitamin C, protein) (Baenas et al., 2015; Xie et al., 2018). Owing to its short growing period, this plant species has also proven to be a valuable model system for addressing the effects of engineered nanoparticles on edible parts of the plants (Zuverza-Mena et al., 2016). For this study, seeds of *R. sativus* cultivar Trailblazer F1 charito were purchased from Hezhiyuan Seed Company (China), a variety commonly used in China. Seeds were surface-sterilized in 10% H_2O_2 (v/v) for 30 min, washed and then soaked in sterile distilled water for 12 h before being germinated on damp gauze at 25 ℃ for 3 days. Equally-sized radish seedlings were transplanted into ceramic pots (15 cm diameter, and 18 cm high) in a climate chamber (25 °C, 55 ± 5% RH, 16 h/8 h (day/night), 12,000 LX of active radiation). Each ceramic pot contained 1/4 strength of Hoagland nutrient solution (pH = 6.8, mmol L^{-1}): K_2SO_4, 0.75; $Ca(NO_3)_2$, 2.0; KCl, 0.1; KH_2PO_4, 0.25; $MgSO_4.7\ H_2O$, 0.65; H_3BO_3, 1.0×10^{-3}; $MnSO_4{\cdot}H_2O$, 1.0×10^{-3}; $ZnSO_4.7\ H_2O$, 1.0×10^{-3}; $CuSO_4.5\ H_2O$, 1×10^{-4}; $(NH_4)_6Mo_7O_{24}$, 5×10^{-6}; Fe-EDTA, 0.1 (Wang et al., 2012). During a preliminary experiment, we observed that 0.76 mg L^{-1} La^{3+} were released from 300 mg L^{-1} La_2O_3 NPs in deionized water in the presence of radish seedling after exposure for 48 h, and the growth of radish seedling was not significantly influenced (Fig. S2). Therefore, ionic control (0.8 mg L^{-1} La^{3+}) was set to test the ionic phytotoxicity in this study. After 25 days, when the taproots began to swell, the radish seedlings were transferred into the liquid solutions of La_2O_3 NPs of different concentrations (0, 10, 50, 100 and 300 mg L^{-1} La_2O_3 NPs, hereafter referred to CK, NP10, NP50, NP100, NP300 for simplicity), and grown hydroponically for 6 days, a time when several radish storage roots started cracking. In order to test the nano-specific effects of La_2O_3 NPs, similar-size radish seedlings were transferred into 300 mg L^{-1} La_2O_3 BPs (BP) and 0.8 mg L^{-1} La^{3+} suspension/solution, serving as the controls of La_2O_3 buck particles and La ion. Each treatment had six replicates. During 6-days exposure period, the La_2O_3 NP suspension was changed every 48 h in order to exclude the contribution of La^{3+} to the phytotoxicity.

After six days of exposure treatment, leaf chlorophyll concentration (SPAD value) was measured in actively-growing leaves using a Chlorophyll Meter (SPAD-502 plus, Konica Minolta Inc., Japan) before

destructive sampling. Additional photosynthesis-related parameters, including net photosynthetic rate (Pn), stomatal conductance (Gs), transpiration rate (E) and intracellular CO_2 concentrations (Ci), were measured using the CIRAS-3 portable gas exchange system (CIRAS-3, PP-Systems, USA). Next, the plants were harvested and separated into three sections: fine root, storage root and shoots. The fine roots and storage root were gently rinsed with 20 mM EDTA-Na_2 solution (five times) to avoid possible attachment of La_2O_3 NPs (Wang et al., 2012). The whole storage root was divided into two parts with a precision knife: root peel and flesh. The dry biomass was measured after oven-drying at 70 °C for 48 h. Part of the fine roots, leaves, root peel and flesh tissues were then acid-digested completely using a microwave digestion system (MARS 6, CEM, USA), and the contents of total La in leaves, fine and storage root tissues were quantified using ICP-MS (Thermo Fisher, Germany) (Liu et al., 2020). The quality assurance/QC was run as the above-mentioned determination methodology of the La^{3+} release from the La_2O_3 NP suspensions. The remaining epidermis and xylem parenchyma tissues of radish storage roots were separated and immediately frozen in liquid nitrogen and stored at −80 °C for further cell wall component and transcriptome analyses. In order to observe the changes of storage root epidermis tissues in response to La_2O_3 NPs exposure, samples were prepared using the paraffin method as described by Yue et al. (2019), and imaged on a confocal laser scanning microscopy (CLSM, Nikon, A1, Japan) at 488 nm excitation.

2.3. Analysis of cell wall components of storage roots

To observe changes in cell wall composition of radish storage roots after La_2O_3 NP exposure, the cell wall components were extracted as described by Huang et al. (2020). Briefly, 100 mg storage root epidermis and xylem parenchyma tissue samples were separately ground to homogenized powder in liquid nitrogen and added with 1.5 mL of ice-cold ethanol for extraction at room temperature for 30 min. The samples were centrifuged at 10,000 g for 5 min to discard the supernatant. The tubes were rinsed twice with 1.5 mL 80% ethanol and the remaining precipitate was then added with 1.5 mL ice-cold acetone, methanol-chloroform (1:1, v/v) and methanol. The precipitate, corresponding to the crude solution of cell wall, was freeze-dried overnight. Afterwards, the crude cell wall solution was added with 7 mL 0.5% ammonium oxalate buffer solution (including 0.1% $NaBH_4$) (pH 4), boiled in water for 1 h and the supernatant containing pectin was separated by centrifugation at 10,000 g for 5 min. The pectin extraction was repeated twice. After washing three times with distilled water, the precipitate was added in 0.5 mL 4% KOH with 0.1% $NaBH_4$, and the supernatant containing hemicellulose 1 was separated by centrifugation at 10,000 g for 5 min, and then neutralized by acetic acid. The extraction of hemicellulose 1 was repeated three times in 24 h at room temperature. Then, 0.5 mL mixed solution (24% KOH and 0.1% $NaBH_4$) was added to the sediment after the extracting hemicellulose 1 as mentioned above to react at room temperature, the supernatant containing hemicellulose 2 was separated by centrifugation at 10,000 g for 5 min, and neutralized with acetic acid. The extraction of hemicellulose 2 was repeated three times in 24 h. The resulting residue was subsequently washed with distilled water and freeze-dried to obtain the cellulose fraction (Huang et al., 2020). Finally, the obtained supernatants and residues were treated individually by the phenol-sulfuric acid method using glucose as standard to assay the contents of cell wall neutral sugar at a wavelength of 490 nm (Dubois et al., 1956). Root sucrose content was determined according to the method described by Feng et al. (2019).

2.4. RNA-seq measurements

RNA extraction, mRNA purification and sequencing were performed as described by Nagalakshmi et al. (2008) and Yang et al. (2018). The RNA was extracted from the epidermis and xylem parenchyma tissues of radish storage roots. To avoid genomic DNA contamination, RNA samples were treated with RNase-free DNase I (Takara, Japan). The concentration and integrity of RNA were quantified with a NanoDrop2000 spectrophotometer (Thermo Scientific, USA) and an Agilent 2100 Bioanalyzer System (Agilent Technologies, USA). cDNA library was constructed for sequencing on the DNBseq platform, following a probe-anchor synthesis sequence method (BGI, China).

Raw reads generated by DNBseq platform were initially processed to get clean reads by discarding the reads with adaptor contamination, masking low-quality reads. A total of 55.1 gigabase-pairs (Gbps) of data were obtained. Then, transcriptome de novo assembly was carried out using the Trinity platform (Grabherr et al., 2011). The assembled clean reads were clustered and this eliminated any redundancy in obtaining unigenes using the TIGR Gene Indices clustering tools (TGICL) (Pertea et al., 2003). Finally, the obtained unigenes were referred to as "All-Unigenes" and clustered into the following two parts: one part included clusters of several unigenes sharing $\geq$ 70% sequence similarity with each other (starting with "CL," followed by the gene family ID), the other part included singletons (starting with "Unigene"). To identify differential expression genes (DEGs) between the two different samples, the gene expression levels were calculated using the fragments per kilobase of exon per million mapped reads (FRKM) method (Mortazavi et al., 2008). A Venn diagram was used to show logical relationships among the DEGs between groups (http://bioinfogp.cnb.csic.es/tools/venny/index.html). Cufflinks tool (http://cufflinks.cbcb.umd.edu/) was employed to quantify differential expression analysis (Trapnell et al., 2013). Gene expression data was analyzed by first applying a threshold for false discovery rate (FDR) < 0.05, and then a fold change ≥ 2 was used to determine significant differences across treatments. Additionally, functional-enrichment analyses, including GO and KEGG were performed to identify which DEGs were significantly enriched in GO terms and metabolic pathways when their Bonferroni-corrected P-value was less than 0.05 (Young et al., 2010; Xu et al., 2019).

2.5. Validation of DEG expression with quantitative real-time PCR (qPCR)

To verify the transcriptomic data, the samples were analyzed via qPCR in accordance with previously-described methods (Xiao et al., 2016). Briefly, additional RNA was isolated from the epidermis and xylem parenchyma tissues as described above. For qPCR analysis, primers for unigenes involved in the biosynthesis of pectin (CL469. Contig1_All, CL7407. Contig7_All and Unigene20023_All) and IAA (CL3618. Contig4_All, Unigene2606_All, CL6699. Contig2_All) were designed using Primer BLAST (https://www.ncbi.nlm.nih.gov/tools/primer-blast/ index.cgi) and synthesized by the Sangon Biotech Co., Ltd (Shanghai, China) (Table S3). UP2 was selected as the internal control gene (Duan et al., 2017). qPCR was performed on a CFX 96 touch Real Time PCR System platform (BioRad, USA) using the UltraSYBR Mixture (CWBIO, China) following the manufacturer's instructions and qPCR protocol was according to a previous report (Liu et al., 2020). Sequentially, the relative gene expression was calculated using the comparative CT method with the formula Relative Quantification (RQ) $= 2^{-\Delta\Delta CT}$ (Livak and Schmittgen, 2001). All reactions were performed in triplicate, and the data were analyzed using the Bio-Rad CFX Manager software.

2.6. Data analysis

All statistical analyses were performed with the R software v3.3.2 (R Development Core Team, 2016). Data were expressed as means ± standard error (SE) (n = 6 replicates per treatment). After the normality and homogeneity tests, the effect of La_2O_3 NPs on radish growth performance, root cell wall composition, photosynthetic parameters and La concentration was respectively examined using a one-way ANOVA with raw data. Differences within treatments were determined by Tukey's

post-hoc tests ($p < 0.05$).

3. Results and discussion

3.1. Radish growth after exposure to La_2O_3 NPs

Growth parameters of radish were determined upon exposure of La_2O_3 NPs, La_2O_3 BPs and La^{3+} for six days (Fig. 1). The radish shoot biomass was decreased by the La_2O_3 NPs treatments, particularly at the dose of 300 mg L^{-1} (Fig. 1a), while no significant changes were observed in the fine root biomass across all treatments (Fig. 1b). La_2O_3 NPs exposure at 10 mg L^{-1} (NP10) concentration increased the storage root biomass by 18%, while La_2O_3 NPs exposure with the higher concentrations, such as NP50, NP100 and NP300, decreased the storage root biomass by 8%, 38% and 60%, respectively (Fig. 1c). Moreover, La_2O_3 NPs exposure at, or above 50 mg L^{-1} tended to decrease the radish storage root flesh, peel biomass, and the ratio of flesh and peel biomass (Fig. 1d–f). Particularly, the NP100 treatment decreased the flesh biomass, peel biomass and ratio of flesh and peel biomass by 44.7%, 16.7% and 29.0%, respectively, and the strongest inhibition effect on radish storage root development was significantly visible at the highest concentration of La_2O_3 NPs (NP300) (Fig. 1d–f). Finally, the NP100 and NP300 treatment markedly resulted in radish root cracking (Fig. S3). In this study, as compared to the 300 mg L^{-1} of La_2O_3 BPs treatment, the equivalent dose of La_2O_3 NPs suspension reduced more storage root biomass, indicating that La_2O_3 NPs displayed a strong nano-specific toxicity effect on radish edible root growth. Moreover, given that the all above radish growth parameters showed no significant differences between the control and La^{3+} treatment (Fig. 1), we can conclude that the toxicity of La_2O_3 NPs on radish growth was not driven by the La^{3+} release from the La_2O_3 NPs in this case.

Recent studies have demonstrated that La_2O_3 NPs could induce both beneficial and detrimental effects in terrestrial plants, as measured by physiological, biochemical, and molecular variables (Yue et al., 2019). Photosynthesis is an essential metabolic process and provides more than 75% of photosynthates that are translocated to stem and root system for plant growth and development (Shiroya et al., 1962). Thus, the observed reduced storage root biomass could be the result of decreased photosynthesis imposed by La_2O_3 NPs exposure. At low La_2O_3 NPs concentration (NP10), or by La^{3+} treatment, the photosynthesis parameters Pn, Gs, E and Ci of radish plants were not significantly different than those of control plants, but were significantly inhibited by La_2O_3 NPs when the exposure dose was more than 100 mg L^{-1} (Fig. 2). Particularly, NP100 and NP300 treatment notably decreased the Pn of radish plants by 18.9% and 32.0%, respectively (Fig. 2a). Consistent with this, leaf chlorophyll content was also greatly reduced in NP100 and NP300-treated radish leaves (Fig. S4a), suggesting that La_2O_3 NPs-mediated reduction in photosynthesis is caused by the reduced photosynthetic pigment contents. Similarly, after La_2O_3 NP exposure, obvious decreases were observed for other gas exchange parameters including Gs, E and Ci, particularly in the presence of 300 mg L^{-1} La_2O_3 NPs (Fig. 2b–d). These results are in line with previous studies that confirmed the negative effects of metal NPs on the photosynthesis and gas exchange parameters of *Oryza sativa* (Abbas et al., 2019) and *Arabidopsis thaliana* (Wang et al., 2016). Therefore, the observed negative effects of La_2O_3 NPs on radish are likely caused by the reduced chlorophyll content and photosynthesis-related gas exchange parameters in leaves, which in turn limited photosynthesis, and thus reduced the storage root biomass accumulation. However, the phytotoxic effect of La_2O_3 NPs on radish plants may be different from those of other rare earth element nanoparticles such as CeO_2 NPs. Indeed, previous study reported that radish soil exposure with 100 mg Kg^{-1} CeO_2 NPs had no inhibition on photosynthesis, and even significantly increased the leaf chlorophyll content, which might have been driven by increased anti-oxidative enzyme activities in the roots and leaves (Gui et al., 2017). Altogether, these results suggest rare earth element NPs-specific

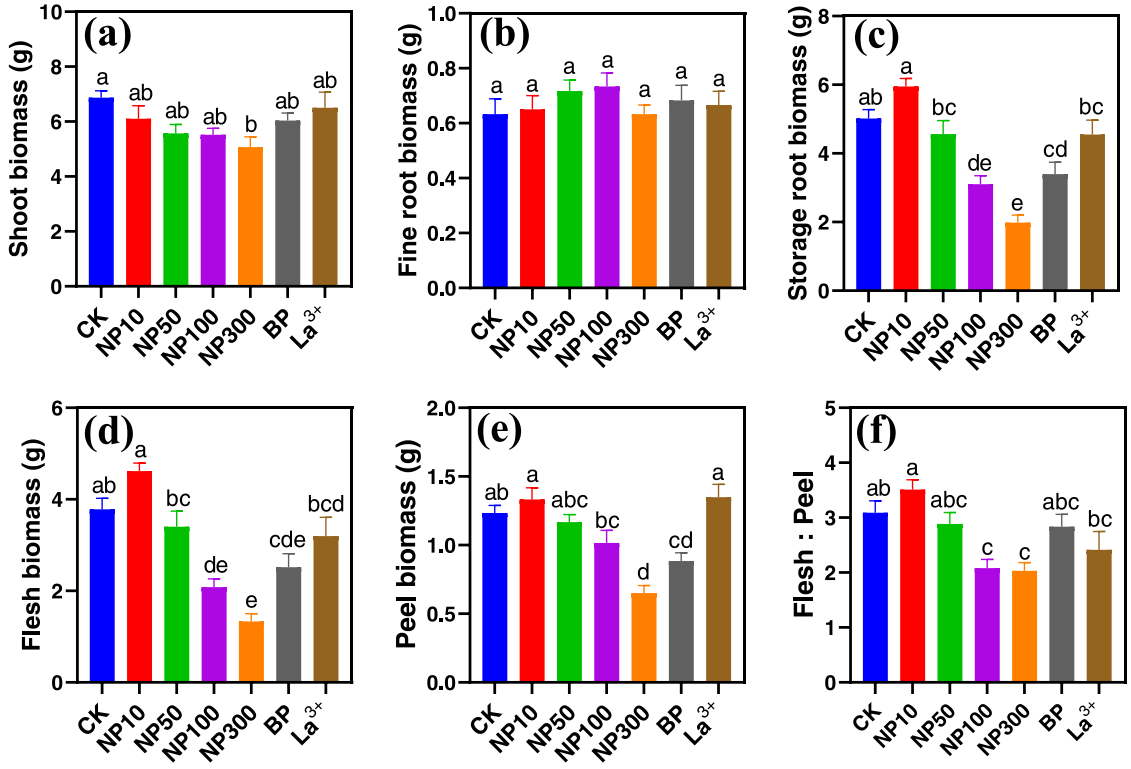

Fig. 1. Growth parameters of radish exposed to different concentrations of La_2O_3 NPs for 6 days. (a) Shoot biomass, (b) fine root biomass, (c) storage root biomass, (d) storage root flesh biomass, (e) storage root peel biomass (f) ratio of storage root flesh and peel biomass. Data are means ± SE (n = 6). La treatments: CK, control without La_2O_3 NPs; NP10, 10 mg L^{-1} La_2O_3 NPs; NP50, 50 mg L^{-1} La_2O_3 NPs; NP100, 100 mg L^{-1} La_2O_3 NPs; NP300, 300 mg L^{-1} La_2O_3 NPs; BP, 300 mg L^{-1} La_2O_3 bulk particles; La^{3+}, 0.8 mg L^{-1} La ion. Different letters indicate significant difference among La treatments (Tukey's HSD test, $p < 0.05$).

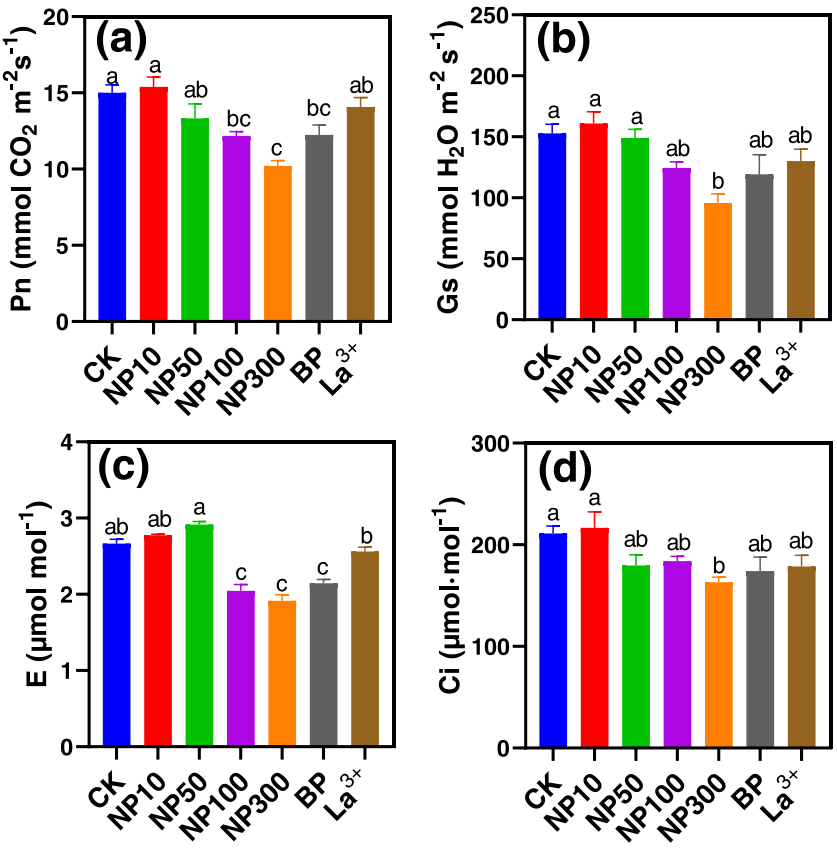

Fig. 2. The gas exchange parameters: (a) net photosynthetic rate (Pn), (b) stomatal conductance (Gs), (c) transpiration rate (E) and (d) intracellular CO_2 concentrations (Ci) and of radish in response to La_2O_3 treatments for 6 days. Data are means ± SE (n = 6). La treatment labels as Fig. 1. Different letters indicate significant difference among La treatments (Tukey's HSD test, $p < 0.05$).

effects on plants, and call for further comparative studies.

3.2. La uptake and internalization in radish plant tissues

We observed that the concentration of La in leaves and particularly in roots increased with the increasing dose of La_2O_3 NPs (from 10 to 300 mg L^{-1}) (Fig. 3a and b). Compared with that in control plants, NP100, NP300 and BP treatment significantly increased La content in radish leaves (Fig. 3a), and all the tested treatments except La^{3+} notably increased the La content in radish fine roots (Fig. 3b). In terms of radish edible organs, La concentration in root peel and flesh tissues of storage roots exposed to La_2O_3 NPs at the dose of 50, 100 and 300 mg L^{-1} was much higher than those treated with La_2O_3 BPs, La^{3+} and control (Fig. 3c and d). The La contents in radish edible tissues peel and flesh increased in a dose-dependent manner (Fig. 3c and d). Similar dose-dependent effects were observed in peanut (*Arachis hypogaea* L.), in which 50 and 500 mg kg^{-1} CuO NPs soil addition resulted in an increase of 88% and 163% Cu concentration in the grains, respectively (Rui et al., 2018). Moreover, we also found that the concentration of La in root peel tissues was much higher than that in flesh tissues at the same exposure concentration of La_2O_3 NPs (Fig. 3c and d), which was likely due to the adsorption of La_2O_3 NPs on the epidermal cell of the storage root. Similarly, a recent study also found that the accumulation of Cerium (Ce) element was principally in the radish taproot peel, with significantly lower Ce concentration in the edible flesh after soil CeO_2 NPs exposure (Zhang et al., 2017a, 2017b). Therefore, these results suggest that a primary pathway for La accumulation in radish storage roots was physical adsorption on the surface and radial diffusion toward the center. Moreover, previous studies suggested that metal NPs can pass through the root epidermis to accumulate in the roots, and then translocate to the shoots through the xylem (Wang et al., 2012). Here, the concentration of La in fine roots was also much higher than that in leaves, which was consistent with other studies (Liu et al., 2020). This observation suggests that less La_2O_3 NPs was possibly translocated from roots to shoots. The reason could be that part of the positively charged NPs absorbed and accumulated in the root cells (Wu et al., 2017), or absorbed in large quantities by negatively charged xylem (White, 2012).

3.3. Root cell wall composition and sugar metabolism in response to La_2O_3 NPs

As predicted, we observed La_2O_3 NPs-mediated changes in cell wall composition of storage root epidermis and xylem parenchyma tissues (Fig. 4). Specifically, NP10, NP50, BP and La^{3+} treatments did not significantly change the cell wall pectin content of epidermis and xylem parenchyma tissues, NP100 significantly decreased cell wall pectin content of epidermis and xylem parenchyma tissues by 16.7% and 12.9%, respectively. Such inhibitory effect was even more visible for the NP300 treatment, and again stronger in the epidermis tissues (Fig. 4a), suggesting that La_2O_3 NPs exposure induced much stronger inhibition on cell wall pectin synthesis in epidermis tissues than that in xylem parenchyma tissues. The possible explanation for this result is that the La_2O_3 NPs exposure resulted in the inhibition of photosynthetic activity, followed by a reduced net photosynthesis and product assimilation, such as decrease in sucrose which usually can be transported from "source" to "sink" organs in higher plants (Farrar et al., 2000; Ruan, 2012) and involves in the synthesis of other essential metabolite compounds such as starch, cellulose, pectin and proteins (Ruan, 2014). In this study, La_2O_3 NPs exposure at, or above, the dose of 100 mg L^{-1} notably decreased sucrose content more in root epidermis tissues than that in the xylem parenchyma tissues (Fig. S4b). While all the tested treatments did not significantly change the cell wall cellulose content of root xylem

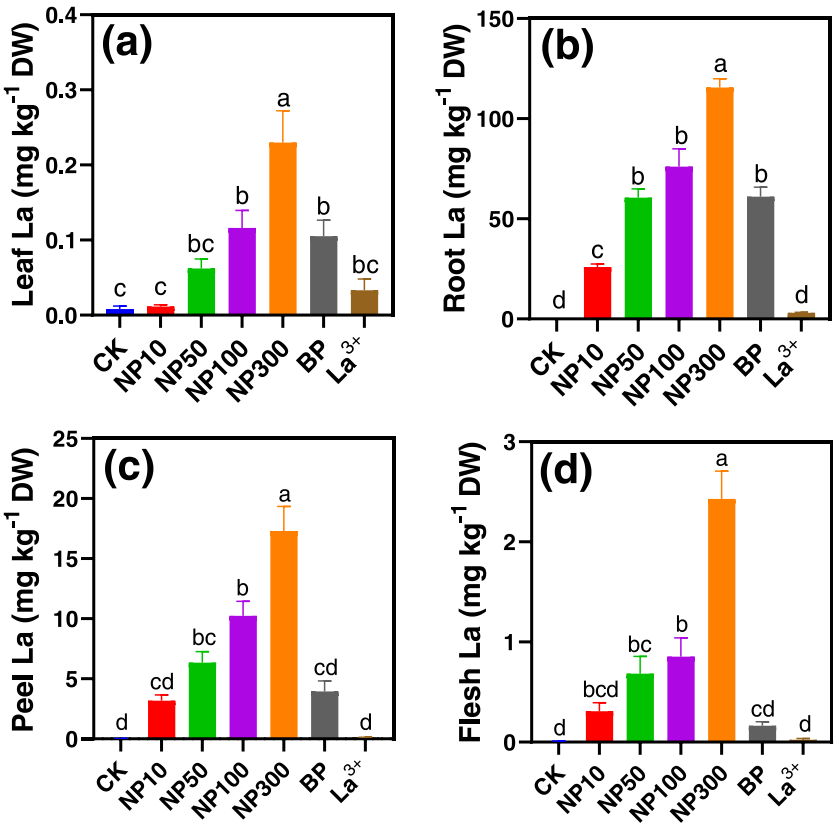

Fig. 3. La concentration in radish plant (a) leaf, (b) fine root, storage root (c) peel and (d) flesh tissues after La_2O_3 NPs exposure. Data are means ± SE (n = 6). La treatment labels as Fig. 1. Different letters among bars indicate statistically significant differences among La treatments (Tukey's HSD test, $p < 0.05$).

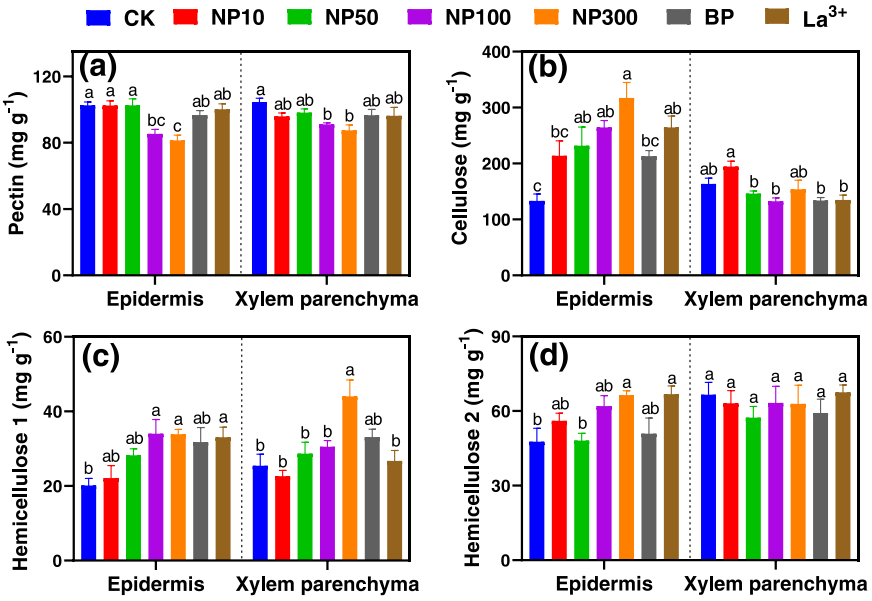

Fig. 4. Change of cell wall components of storage root epidermis and xylem parenchyma tissues in response to La_2O_3 NPs exposure. (a) Pectin, (b) cellulose, (c) hemicellulose 1 and (d) hemicellulose 2. Data are means ± SE (n = 6). La treatment labels as Fig. 1. Different letters among bars indicate statistically significant differences in cell wall polysaccharides of in epidermis or xylem parenchyma tissues among La treatments (Tukey's HSD test, $p < 0.05$).

parenchyma tissues, NP50, NP100, NP300 and La^{3+} treatment significantly increased cell wall cellulose content of epidermis tissues (Fig. 4b). Similarly, NP100 and NP300 treatment also increased cell wall hemicellulose 1 content of root epidermis tissues obviously, but only NP300 treatment significantly increased cell wall hemicellulose 1 content of root xylem parenchyma tissues by 42.2% (Fig. 4c). Besides, treatments of NP300 and La^{3+} significantly increased cell wall hemicellulose 2 content of root epidermis tissue, but all the tested treatments did not significantly change the cell wall hemicellulose 2 content of root xylem parenchyma tissues (Fig. 4d). It is well known that the mechanical properties of cell wall, including viscosity and elasticity, are dependent on the content and structure of cell wall components, a variable

composite mixture of cellulose, hemicellulose, and proteins embedded in a matrix of pectin (Cosgrove, 2005; Sun et al., 2016). Hence, it is suggested that the viscosity and elasticity of radish storage root cell walls were disturbed by La_2O_3 NPs exposure particularly at the higher exposure doses, via significantly changing the ultrastructure and composition of cell walls (Fig. S7).

A recent study found that CuO NPs exposure decreased the contents of *Arabidopsis thaliana* root cell wall pectin (including esterified uronic acid and nonesterified uronic acid) but increased cell cellulose contents (Nie et al., 2020). Similarly, in the present study, La_2O_3 NPs exposure decreased the cell wall pectin content but increased the cell wall cellulose content especially in root epidermis tissues. It is well known that cellulose microfibrils provide tensile strength to the cell wall and determine the directionality of cell expansion, and they are usually interlinked by hemicelluloses, possibly at mechanical hotspots, and embedded within a pectin matrix (Verbančič et al., 2018). A previous study also found that fruit cell walls with less water-soluble and more ionically and covalently-bound pectins finally reduced the elasticity of cell wall microfibrils and induced cracking (Jiang et al., 2019). Indeed, the confocal microscopy images of storage root epidermis tissues indicated that plant cell were damaged, and particularly the cell adhesion were disrupted severely after 100 mg L^{-1} La_2O_3 NP exposure (Fig. S7). It has been reported that metal oxide nanoparticle exposure at high dose induced the production of ROS including hydroxyl radicals (·OH) (Yue et al., 2018), and the·OH radicals are very reactive so that they can act as scissors to breakdown pectin-polysaccharide networking polymers in the cell walls (Kim et al., 2019). Besides, soil inadequate watering and water status were reportedly essential factors that increase radish root cracking (Wan and Kang, 2006). However, given that radish plants grew in the hydroponic condition, the water status in the growth medium was not the main factor affecting root cracking in this study. Thus, the decreased pectin concentration in cell walls of storage root epidermis tissues caused loosening of the tethers between cellulose microfibrils, and the disruption of plant cell adhesion, which ultimately made the epidermis tissue to lose its elasticity, and likely facilitated root cracking.

3.4. *Transcriptomic analysis revealed differential responses to La_2O_3 NPs exposure*

In this study, based on the comparisons of radish plant physiological changes including plant growth performance, photosynthesis and root cracking among the treatments of 300 mg L^{-1} La_2O_3 NPs, equivalent bulk La_2O_3 and ionic La, we could clearly conclude that the La_2O_3 NPs do have nano-specific toxicity on radish growth and caused root cracking phenomenon but bulk La_2O_3 do not. Moreover, given our initial observations that 100 mg L^{-1} was the lowest observed La_2O_3 NPs exposure concentration for causing clear root cracking along with significant changes in taproot growth and cell wall components, 100 mg L^{-1} was chosen as the exposure concentration to further investigate the La_2O_3 NPs-mediated molecular mechanisms of cell wall polysaccharide synthesis for the interpretation of root cracking. Thus, we here present mRNA sequencing data on transcriptome impacts to radish plants during their tuber expansion following six days of 100 mg L^{-1} La_2O_3 NPs exposure, as compared to control. The number of filtered differentially expressed genes (DEGs) is shown in Fig. 5(a). Overall, compared to control plants, 1485 genes (832 up-regulated and 653 down-regulated) were differentially expressed in storage root epidermis tissues after La_2O_3 NPs exposure, and 1780 genes (949 up-regulated and 831 down-regulated) were differentially expressed in storage root xylem parenchyma tissues after La_2O_3 NPs exposure (Fig. 5a). Compared the DEGs between root epidermis and xylem parenchyma tissues, 1474 (320 up-regulated and 1154 down-regulated) and 906 (247 up-regulated and 659 down-regulated) DEGs were identified in the absence and presence of La_2O_3 NPs exposure, respectively (Fig. 5a). In accordance with the Venn diagram analysis (Fig. 5b), 508, 788, 1034 and 502 genes were specifically differentially expressed in the comparisons of the group of epidermis tissues after La_2O_3 NPs exposure (abbreviated as "EP_CK-vs-EP_NPs"), the group of xylem parenchyma tissues after La_2O_3 NPs exposure (abbreviated as "XP_CK-vs-XP_NPs"), the group of difference between epidermis and xylem parenchyma tissues in the absence of La_2O_3 NPs exposure (abbreviated as "EP_CK-vs-XP_CK"), and the group of difference between epidermis and xylem parenchyma tissues in the presence of La_2O_3 NPs exposure (abbreviated as "EP_NPs-vs-XP_NPs"), respectively (Fig. 5b).

On the basis of the DEG results, we performed gene ontology (GO) enrichment analysis (Fig. S5). GO analysis indicated that most DEGs in La_2O_3 NPs-treated radish root epidermis and xylem parenchyma tissue were enriched for cellular process, cell part and binding (Fig. S5a and b). To understand the functions of the DEGs, their KEGG pathway enrichment of radish root epidermis and parenchyma tissues upon La_2O_3 NPs treatment was also analyzed. The top 20 KEGG pathways with the highest number of DEGs are shown in (Fig. 6), in which ubiquinone and other terpenoid-quinone biosynthesis (ko00130), N-Glycan biosynthesis (ko00510), amino sugar and nucleotide sugar metabolism (ko00520) were enriched in root epidermis tissues after La_2O_3 NPs exposure (Fig. 6a), and nitrogen metabolism (ko00910), alpha-linolenic acid metabolism (ko00592) and glucosinolate biosynthesis (ko00966) were notably enriched in root xylem parenchyma tissues after La_2O_3 NPs exposure (Fig. 6b). Particularly, 920 DEGs were differentially expressed in both root epidermis and xylem parenchyma tissues after La_2O_3 NPs

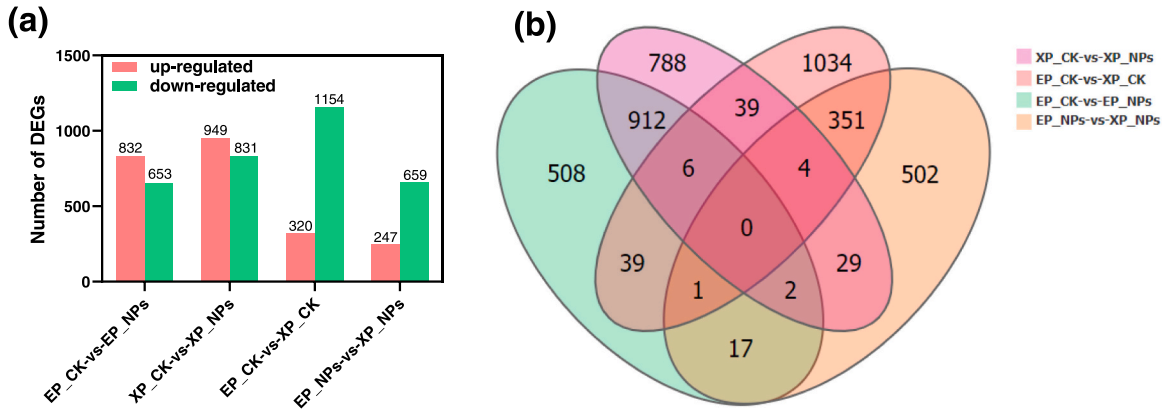

Fig. 5. Overview of differential gene expression under different treatments. (a) Numbers of differentially expressed genes (DEGs) between each group. (b) Venn diagram showing the number of significant DEGs in each group. EP_CK-vs-EP_NPs: group of epidermis tissues after La_2O_3 NPs exposure; XP_CK-vs-XP_NPs: group of xylem parenchyma tissues after La_2O_3 NPs exposure; EP_CK-vs-XP_CK: group of the comparison between epidermis and xylem parenchyma tissues without La_2O_3 NPs exposure; EP_NPs-vs-XP_NPs: group of the comparison between epidermis and xylem parenchyma tissues with La_2O_3 NPs exposure.

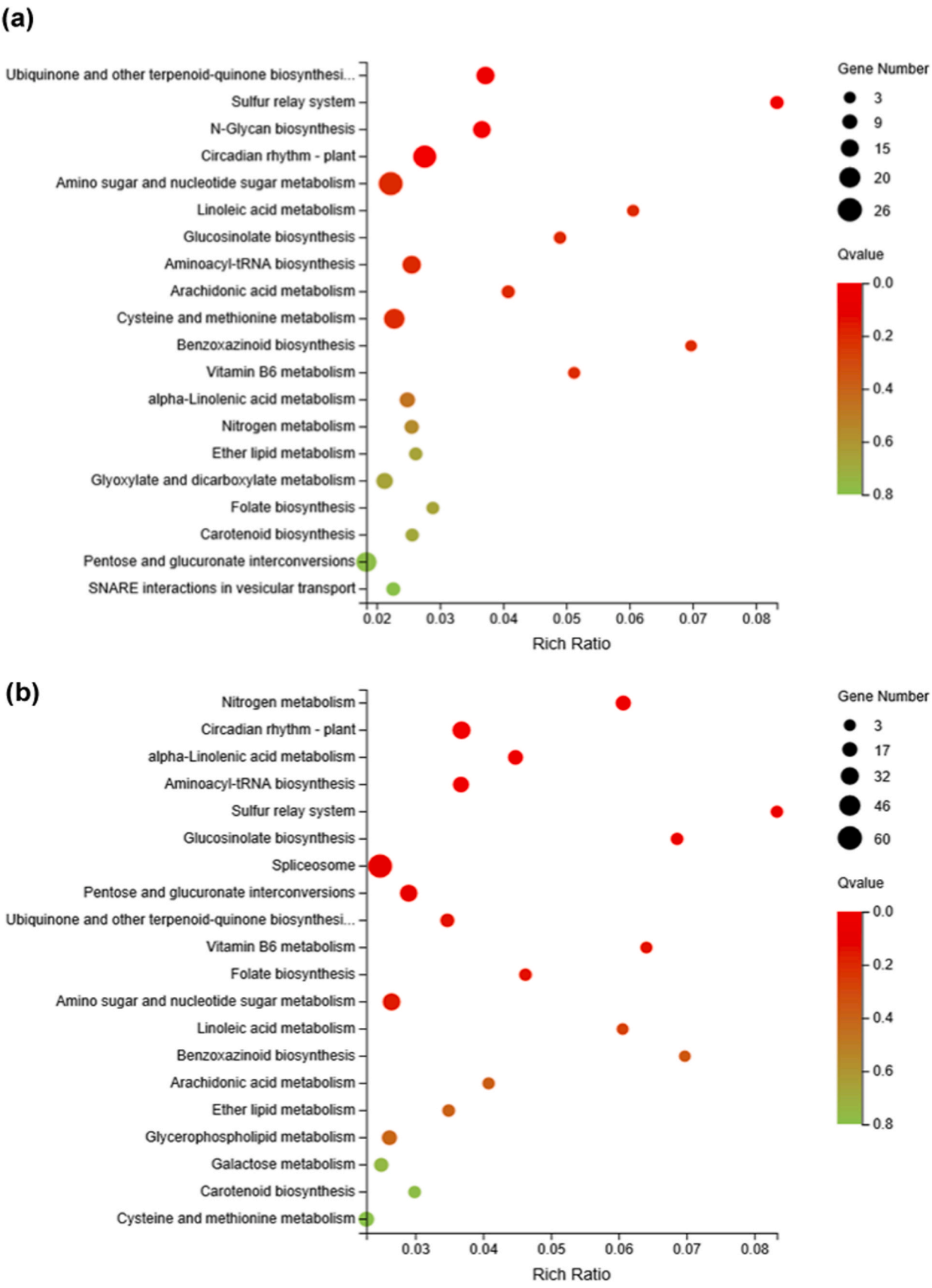

Fig. 6. Top 20 pathways of KEGG enrichment of differentially expressed genes (DEGs) in radish storage root epidermis (a) and xylem parenchyma (b) tissues in response to La_2O_3 NPs exposure. The rich factor is the percentage of DEGs out of the total number of detected genes in the pathway. Coloring indicates Q-value with higher in green and lower in red. The lower Q-value indicates the more significantly enriched. Bigger dots indicate higher numbers of DEGs. (For interpretation of the references to colour in this figure legend, the reader is referred to the web version of this article)

exposure (Fig. 5b), and their KEGG pathway enrichment was further analyzed: the pathway of amino sugar and nucleotide sugar metabolism (ko00520), vitamin B6 metabolism (ko00750), and nitrogen metabolism (ko00910) were enriched (Fig. S6). It has been reported that bioavailable nitrogen is a key factor in enhancing crop production and photosynthesis (Makino, 2011; Zhang et al., 2017a, 2017b). In this study, 8 DEGs related to the nitrate/nitrite transporter (i.e., CL9019. Contig2_All, Unigene20503_All, Unigene6828_All, Unigene6852_All and Unigene6858_All) and glutamate synthase (i.e., CL13367. Contig2_All, CL13367. Contig6_All and CL13367. Contig7_All) in the nitrogen metabolism pathway were all up-regulated after La_2O_3 NPs exposure (Table S4), suggesting that La_2O_3 NPs-driven increase in nitrogen metabolism was not the main limiting factor of radish growth and photosynthesis. However, most genes involved in amino sugar and nucleotide sugar metabolism pathway (ko00520), especially for pectin biosynthesis (i.e., CL469. Contig1_All, CL7407. Contig7_All and Unigene20023_All), were down-regulated in both root epidermis and xylem parenchyma tissues after La_2O_3 NPs exposure (Fig. 7). It has been reported that the newly fixed carbon, in the form of UDP-glucose and other nucleotide sugars derived from UDP-glucose, contributes to the synthesis of cell wall polysaccharides i.e., cellulose, and pectin and hemicelluloses (Verbančič et al., 2018). While the starch and sucrose metabolism (ko00910) was not significantly enriched among the top 20 KEGG pathways, 13 DEGs related to the starch and sucrose metabolism were identified (Table S4), 5 of which involved in the biosynthesis of cellulose (i.e., Unigene16368_All, CL11759. Contig3_All, CL1298. Contig4_All, CL8246. Contig7_All and Unigene5966_All) were up-regulated by La_2O_3 NPs exposure (Table S4), which could be the reason why the cell wall cellulose content in root epidermis and xylem parenchyma tissues increased after La_2O_3 NPs exposure.

Dysfunctions in the plant hormones' signal transduction pathways have also been associated with fruit cracking in some fruits, as for example in sweet cherries (Cline and Trought, 2007). In this study, 26 DEGs involved in plant hormone signal transduction pathway (ko04075) after La_2O_3 NPs treatment were identified. Particularly, the unigenes involved in the biosynthesis of auxin (i.e., ARF: CL3618. Contig4_All, Unigene2606_All; SAUR: CL6699. Contig2_All) were down-regulated in both root epidermis and parenchyma tissues of the La_2O_3 NPs-treated plants (Fig. 7a and b, Table S4). This results contrast with the general observation that the biosynthesis and transport of auxin is highly involved in root growth and development (Saini et al., 2013). Moreover, La_2O_3 NPs exposure down-regulated the DEGs involved in the biosynthesis of cell wall pectin and IAA, which directly inhibited the coupled processes of root cell wall synthesis and cell enlargement/division. Thus, La_2O_3 NPs pollution could also facilitate root cracking by inhibiting the production of auxin and IAA in root tissues.

3.5. Quantitative real-time PCR validation of DEGs

According to the results described above, six unigenes involved in the biosynthesis of pectin (i.e., GAUT: CL469. Contig1_All and CL7407. Contig7_All; GALE: Unigene20023_All) and IAA (ARF: CL3618. Contig4_All and Unigene2606_All; SAUR: CL6699. Contig2_All) were selected to more accurately compare gene expression patterns after La_2O_3 NPs exposure using qPCR (Table S4). qPCR analysis showed that 100 mg L^{-1} La_2O_3 NPs exposure dramatically down-regulated the expression of unigenes involved in alpha-1,4-galacturonosyltransferase (i.e., CL469. Contig1_All, CL7407. Contig7_All) and UDP-glucose 4-epimerase (Unigene20023_All) of pectin synthesis in both root epidermis and xylem parenchyma tissues (Fig. 7a and b). Similarly, the identified unigenes related to the auxin response factor (ARF: CL3618. Contig4_All, Unigene2606_All) and SAUR family protein (SAUR: CL6699. Contig2_All) all displayed relatively low expression levels in both root epidermis and xylem parenchyma tissues after 100 mg L^{-1} La_2O_3 NPs exposure (Fig. 7a and b). These results indicate that the identified unigenes can indeed provide insights for further dissecting the molecular mechanisms, related to cell wall pectin and IAA biosynthesis, driving the observed radish storage root cracking after La_2O_3 NPs exposure. Metal oxide nanoparticles have been previously shown to directly alter phytohormones in roots (Vankova et al., 2017). For instance, it was shown that Fe_2O_3 NPs decreased the concentration of the growth-promoting hormone IAA in the roots of conventional cotton (Jihe 321) (Van Nhan et al., 2016). Similarly, a recent report has also shown that the IAA content in rice roots with medium nitrogen supply was greatly reduced when plants were added with 100 and 500 mg L^{-1} of CeO_2 NPs suspensions (Wang et al., 2020). However, previous studies showed that changing the level of auxin would alter cytokinin content during root formation (Palni et al., 1988; Mao et al., 2020), several other hormones including ethylene, ABA, and GA are also responsible for root development (Pacifici et al., 2015), and could be altered by metal oxide nanoparticles (Vankova et al., 2017). Thus, system networks of hormone interactions in radish taproot cracking after La_2O_3 NPs exposure needs to be further investigated in future molecular studies.

4. Conclusions and environmental implication

Our results clearly demonstrated that La_2O_3 NPs affected radish storage formation more strongly than La_2O_3 BPs at corresponding concentrations. Physiological analysis showed that the toxicity of La_2O_3 NPs on radish storage root growth is mainly generated through a decrease in photosynthetic parameters, inhibiting cell wall pectin synthesis, disrupting plant cell adhesion and interfering with biosynthesis of IAA which could contribute to cell division and expansion (Fig. 8). GO and

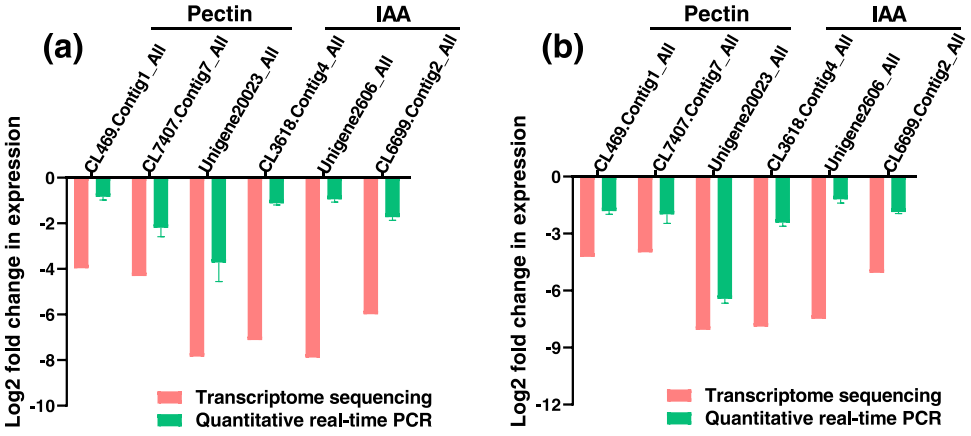

Fig. 7. Expression patterns of genes involved in synthesis of pectin and IAA in root epidermis (a), and xylem parenchyma tissues (b) using transcriptome sequencing (FPKM) and quantitative real-time PCR. Data shown are means ± SE (n = 3).

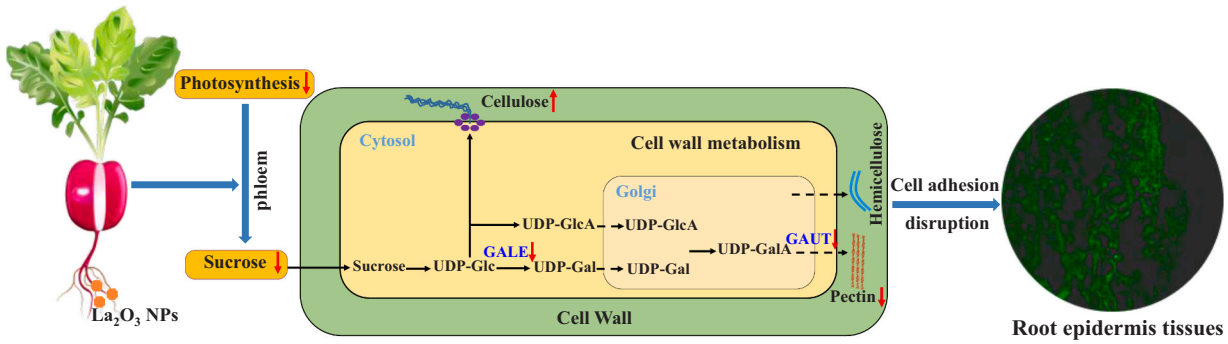

Fig. 8. Molecular mechanism for La_2O_3 NPs-induced synthesis of cell wall polysaccharides and root cracking. Sucrose produced by photosynthesis in source leaves is exported to growing sink organs (storage root) by the phloem. Nucleotide sugars such as uridine diphosphate (UDP) glucose (UDP-Glc) is produced by catabolism of sucrose via sucrose synthase, and are then transported into the Golgi bodies via several nucleotide sugar transporters for synthesis of hemicelluloses and pectins. Significantly expressed transcriptome unigenes involved in regulating pectin biosynthesis were shown in blue. "↑" and "↓" mean La_2O_3 NPs-mediated promoting and inhibiting effects on the carbon supply and regulation of cell wall synthesis of radish plant roots, respectively. Abbreviations: UDP-galacturonate (UDP-GalA); UDP-glucuronic acid (UDP-GlcA); UDP-galactose (UDP-Gal); UDP-galacturonic acid (UDP-GalA); GAUT (alpha-1, 4-galacturonosyltransferase [EC:2.4.1.43]); GALE (UDP-glucose 4-epimerase [EC:5.1.3.2]). (For interpretation of the references to colour in this figure legend, the reader is referred to the web version of this article)

KEGG pathway enrichment analyses showed that several of the 920 identified cracking-related DEGs were involved in amino sugar and nucleotide sugar metabolism, plant hormone signal transduction pathways, and starch and sucrose metabolism, thus providing specific insights for future targeted molecular studies on root cracking. Finally, La_2O_3 NPs exposure at high dose (>100 mg L^{-1}) resulted in root cracking, whereas low dose (10 mg L^{-1}) manifested a slight promotion effect on storage root growth. Therefore, dose-dependent effects of NPs, particularly in the application of nano-agricultural technology in the future, should be clearly addressed. Being aware of disadvantages of hydroponic conditions, such as lacking the effect of the soil matrix on the research and elucidation of the mechanism of nanomaterials-induced root cracking, there is an urgent need to perform more research on actual soil exposure scenario in future. Taken together, this study provides a multi-layered step forward for understanding the causes of NPs phytotoxicity in edible tissues of plants, including the molecular mechanisms related to cell wall carbohydrate metabolism during taproot formation in response to NPs stress.

CRediT authorship contribution statement

Zhenggao Xiao: Conceptualization, Methodology, Formal analysis, Data curation, Writing - original draft, Funding acquisition. **Le Yue:** Resources, Funding acquisition. **Chuanxi Wang:** Methodology, Resources. **Feiran Chen:** Methodology, Investigation, Visualization. **Yin Ding:** Data curation, Investigation, Validation. **Yinglin Liu:** Investigation, Validation. **Xuesong Cao:** Investigation, Visualization. **Zhe Chen:** Visualization. **Sergio Rasmann:** Writing - review & editing. **Zhenyu Wang:** Writing - review & editing, Funding acquisition, Project administration.

Declaration of Competing Interest

All authors declared no conflict of interest.

Acknowledgments

This work was supported by the National Natural Science Foundation of China (41820104009, 41530642, 41807381 and 41807378). We thank Misses Wenqing Zhu, Hanyue Yang and Junfeng Tang, Mr. Weisheng Ma for their kind helps in laboratory analyses.

Appendix A. Supporting information

Supplementary data associated with this article can be found in the online version at doi:10.1016/j.jhazmat.2020.124971.

References

Abbas, Q., Liu, G., Yousaf, B., Ali, M.U., Ullah, H., Ahmed, R., 2019. Effects of biochar on uptake, acquisition and translocation of silver nanoparticles in rice (*Oryza sativa* L.) in relation to growth, photosynthetic traits and nutrients displacement. Environ. Pollut. 250, 728–736.

Baenas, N., Ferreres, F., García-Viguera, C., Moreno, D.A., 2015. Radish sprouts—Characterization and elicitation of novel varieties rich in anthocyanins. Food Res. Int. 69, 305–312.

Balusamy, B., Kandhasamy, Y.G., Senthamizhan, A., Chandrasekaran, G., Subramanian, M.S., Kumaravel, T.S., 2012. Characterization and bacterial toxicity of lanthanum oxide bulk and nanoparticles. J. Rare Earths 30, 1298–1302.

Cline, J.A., Trought, M., 2007. Effect of gibberellic acid on fruit cracking and quality of Bing and Sam sweet cherries. Can. J. Plant Sci. 87, 545–550.

Cosgrove, D.J., 2005. Growth of the plant cell wall. Nat. Rev. Mol. Cell Biol. 6, 850–861.

Duan, M., Wang, J., Zhang, X., Yang, H., Wang, H., Qiu, Y., Song, J., Guo, Y., Li, X., 2017. Identification of optimal reference genes for expression analysis in radish (*Raphanus sativus* L.) and its relatives based on expression stability. Front. Plant Sci. 8, 1605.

Dubois, M., Gilles, K.A., Hamilton, J.K., Rebers, Pt, Smith, F., 1956. Colorimetric method for determination of sugars and related substances. Anal. Chem. 28, 350–356.

Farrar, J., Pollock, C., Gallagher, J., 2000. Sucrose and the integration of metabolism in vascular plants. Plant Sci. 154, 1–11.

Feng, Y.X., Yu, X.Z., Mo, C.H., Lu, C.J., 2019. Regulation network of sucrose metabolism in response to trivalent and hexavalent chromium in *Oryza sativa*. J. Agric. Food Chem. 67, 9738–9748.

Grabherr, M.G., Haas, B.J., Yassour, M., Levin, J.Z., Thompson, D.A., Amit, I., Adiconis, X., Fan, L., Raychowdhury, R., Zeng, Q., Chen, Z., Mauceli, E., Hacohen, N., Gnirke, A., Rhind, N., di Palma, F., Birren, B.W., Nusbaum, C., Lindblad-Toh, K., Friedman, N., Regev, A., 2011. Full-length transcriptome assembly from RNA-Seq data without a reference genome. Nat. Biotechnol. 29, 644–652.

Gui, X., Rui, M., Song, Y., Ma, Y., Rui, Y., Zhang, P., He, X., Li, Y., Zhang, Z., Liu, L., 2017. Phytotoxicity of CeO_2 nanoparticles on radish plant (*Raphanus sativus*). Environ. Sci. Pollut. Res. 24, 13775–13781.

Huang, X., Li, Y., Chen, K., Chen, H., Wang, F., Han, X., Zhou, B., Chen, H., Yuan, R., 2020. NOM mitigates the phytotoxicity of AgNPs by regulating rice physiology, root cell wall components and root morphology. Environ. Pollut. 260, 113942.

Hwang, R., Chang, C.H., Zhu, Y., Xia, T., 2019. Biotransformation and potential adverse effects of rare earth oxide nanoparticles. In: Kumar, C.S.S.R. (Ed.), Nanotechnology Characterization Tools for Environment, Health, and Safety. Springer Berlin Heidelberg, Berlin, Heidelberg, pp. 47–63.

Jiang, F., Lopez, A., Jeon, S., de Freitas, S.T., Yu, Q., Wu, Z., Labavitch, J.M., Tian, S., Powell, A.L.T., Mitcham, E., 2019. Disassembly of the fruit cell wall by the ripening-associated polygalacturonase and expansin influences tomato cracking. Hortic. Res. 6, 17.

Kim, J.H., Kim, D., Seo, S.M., Kim, D., 2019. Physiological effects of zero-valent iron nanoparticles in rhizosphere on edible crop, *Medicago sativa* (Alfalfa), grown in soil. Ecotoxicology 28, 869–877.

Liu, Y., Yue, L., Wang, C., Zhu, X., Wang, Z., Xing, B., 2020. Photosynthetic response mechanisms in typical C3 and C4 plants upon La_2O_3 nanoparticle exposure. Environ. Sci. -Nano 7, 81–92.

Livak, K.J., Schmittgen, T.D., 2001. Analysis of relative gene expression data using real-time quantitative PCR and the $2^{-\Delta\Delta CT}$ method. Methods 25, 402–408.

Lu, V.M., McDonald, K.L., 2020. Lanthanum nanoparticles to target the brain: proof of biodistribution and biocompatibility with adjuvant therapies. Nanomedicine 15, 2107–2117.

Makino, A., 2011. Photosynthesis, grain yield, and nitrogen utilization in rice and wheat. Plant Physiol. 155, 125–129.
Mao, C., He, J., Liu, L., Deng, Q., Yao, X., Liu, C., Qiao, Y., Li, P., Ming, F., 2020. OsNAC$_2$ integrates auxin and cytokinin pathways to modulate rice root development. Plant Biotechnol. J. 18, 429–442.
Ma, Y., Kuang, L., He, X., Bai, W., Ding, Y., Zhang, Z., Zhao, Y., Chai, Z., 2010. Effects of rare earth oxide nanoparticles on root elongation of plants. Chemosphere 78, 273–279.
Ma, Y., Zhang, P., Zhang, Z., He, X., Li, Y., Zhang, J., Zheng, L., Chu, S., Yang, K., Zhao, Y., Chai, Z., 2015. Origin of the different phytotoxicity and biotransformation of cerium and lanthanum oxide nanoparticles in cucumber. Nanotoxicology 9, 262–270.
Mortazavi, A., Williams, B.A., McCue, K., Schaeffer, L., Wold, B., 2008. Mapping and quantifying mammalian transcriptomes by RNA-Seq. Nat. Methods 5, 621–628.
Nagalakshmi, U., Wang, Z., Waern, K., Shou, C., Raha, D., Gerstein, M., Snyder, M., 2008. The transcriptional landscape of the yeast genome defined by RNA sequencing. Science 320, 1344–1349.
Van Nhan, L., Ma, C., Rui, Y., Cao, W., Deng, Y., Liu, L., Xing, B., 2016. The effects of Fe_2O_3 nanoparticles on physiology and insecticide activity in non-transgenic and Bt-transgenic cotton. Front. Plant Sci. 6, 1263.
Nie, G., Zhao, J., He, R., Tang, Y., 2020. CuO nanoparticle exposure impairs the root tip cell walls of *Arabidopsis thaliana* seedlings. Water Air Soil Pollut. 231, 1–11.
Pacifici, E., Polverari, L., Sabatini, S., 2015. Plant hormone cross-talk: the pivot of root growth. J. Exp. Bot. 66, 1113–1121.
Palni, L., Burch, L., Horgan, R., 1988. The effect of auxin concentration on cytokinin stability and metabolism. Planta 174, 231–234.
Pertea, G., Huang, X., Liang, F., Antonescu, V., Sultana, R., Karamycheva, S., Lee, Y., White, J., Cheung, F., Parvizi, B., Tsai, J., Quackenbush, J., 2003. TIGR Gene Indices clustering tools (TGICL): a software system for fast clustering of large EST datasets. Bioinformatics 19, 651–652.
R Development Core Team, 2016. R: A Language and Environment for Statistical Computing. R Foundation for Statistical Computing, Vienna, Austria.
Rizwan, M., Ali, S., Qayyum, M.F., Ok, Y.S., Adrees, M., Ibrahim, M., Zia-Ur-Rehman, M., Farid, M., Abbas, F., 2017. Effect of metal and metal oxide nanoparticles on growth and physiology of globally important food crops: a critical review. J. Hazard. Mater. 322, 2–16.
Ruan, Y.L., 2012. Signaling role of sucrose metabolism in development. Mol. Plant 5, 763–765.
Ruan, Y.L., 2014. Sucrose metabolism: gateway to diverse carbon use and sugar signaling. Annu. Rev. Plant Biol. 65, 33–67.
Rui, M., Ma, C., White, J.C., Hao, Y., Wang, Y., Tang, X., Yang, J., Jiang, F., Ali, A., Rui, Y., Cao, W., Chen, G., Xing, B., 2018. Metal oxide nanoparticles alter peanut (*Arachis hypogaea* L.) physiological response and reduce nutritional quality: a life cycle study. Environ. Sci. Nano 5, 2088–2102.
Saini, S., Sharma, I., Kaur, N., Pati, P.K., 2013. Auxin: a master regulator in plant root development. Plant Cell Rep. 32, 741–757.
Shiroya, T., Lister, G., Krotkov, G., Nelson, C., Slankis, V., 1962. Translocation of the products of photosynthesis to roots of pine seedlings. Can. J. Bot. 40, 1125–1135.
Sisler, J.D., Pirela, S.V., Shaffer, J., Mihalchik, A.L., Chisholm, W.P., Andrew, M.E., Schwegler-Berry, D., Castranova, V., Demokritou, P., Qian, Y., 2016. Toxicological assessment of CoO and La_2O_3 metal oxide nanoparticles in human small airway epithelial cells. Toxicol. Sci. 150, 418–428.
Somerville, C., Bauer, S., Brininstool, G., Facette, M., Hamann, T., Milne, J., Osborne, E., Paredez, A., Persson, S., Raab, T., 2004. Toward a systems approach to understanding plant cell walls. Science 306, 2206–2211.
Sun, C., Lu, L., Yu, Y., Liu, L., Hu, Y., Ye, Y., Jin, C., Lin, X., 2016. Decreasing methylation of pectin caused by nitric oxide leads to higher aluminium binding in cell walls and greater aluminium sensitivity of wheat roots. J. Exp. Bot. 67, 979–989.
De la Torre Roche, R., Servin, A., Hawthorne, J., Xing, B., Newman, L.A., Ma, X., Chen, G., White, J.C., 2015. Terrestrial trophic transfer of bulk and nanoparticle La_2O_3 does not depend on particle size. Environ. Sci. Technol. 49, 11866–11874.
Trapnell, C., Hendrickson, D.G., Sauvageau, M., Goff, L., Rinn, J.L., Pachter, L., 2013. Differential analysis of gene regulation at transcript resolution with RNA-seq. Nat. Biotechnol. 31, 46–53.
Vankova, R., Landa, P., Podlipna, R., Dobrev, P.I., Prerostova, S., Langhansova, L., Gaudinova, A., Motkova, K., Knirsch, V., Vanek, T., 2017. ZnO nanoparticle effects on hormonal pools in Arabidopsis thaliana. Sci. Total Environ. 593–594, 535–542.
Verbančič, J., Lunn, J.E., Stitt, M., Persson, S., 2018. Carbon supply and the regulation of cell wall synthesis. Mol. Plant 11, 75–94.
Wang, Z., Xie, X., Zhao, J., Liu, X., Feng, W., White, J.C., Xing, B., 2012. Xylem- and phloem-based transport of CuO nanoparticles in maize (*Zea mays* L.). Environ. Sci. Technol. 46, 4434–4441.
Wang, X., Yang, X., Chen, S., Li, Q., Wang, W., Hou, C., Gao, X., Wang, L., Wang, S., 2016. Zinc oxide nanoparticles affect biomass accumulation and photosynthesis in *Arabidopsis*. Front. Plant Sci. 6, 1243.
Wang, Y., Zhang, P., Li, M., Guo, Z., Ullah, S., Rui, Y., Lynch, I., 2020. Alleviation of nitrogen stress in rice (*Oryza sativa*) by ceria nanoparticles. Environ. Sci. Nano 7, 2930–2940.
Wan, S., Kang, Y., 2006. Effect of drip irrigation frequency on radish (*Raphanus sativus* L.) growth and water use. Irrig. Sci. 24, 161–174.
White, P.J., 2012. Ion uptake mechanisms of individual cells and roots: short-distance transport. In: Marschner, P. (Ed.), Marschner's Mineral Nutrition of Higher Plants, Third edition.,. Academic Press, San Diego, pp. 7–47.
Wu, B., Zhu, L., Le, X.C., 2017. Metabolomics analysis of TiO_2 nanoparticles induced toxicological effects on rice (*Oryza sativa* L.). Environ. Pollut. 230, 302–310.
Xiao, Z., Liu, M., Jiang, L., Chen, X., Griffiths, B.S., Li, H., Hu, F., 2016. Vermicompost increases defense against root-knot nematode (*Meloidogyne incognita*) in tomato plants. Appl. Soil Ecol. 105, 177–186.
Xie, Y., Xu, L., Wang, Y., Fan, L., Chen, Y., Tang, M., Luo, X., Liu, L., 2018. Comparative proteomic analysis provides insight into a complex regulatory network of taproot formation in radish (*Raphanus sativus* L.). Hortic. Res. 5, 51.
Xu, M.L., Zhu, Y.G., Gu, K.H., Zhu, J.G., Yin, Y., Ji, R., Du, W.C., Guo, H.Y., 2019. Transcriptome reveals the rice response to elevated free air CO_2 concentration and TiO_2 nanoparticles. Environ. Sci. Technol. 53, 11714–11724.
Yang, Y., Wang, F., Wan, Q., Ruan, J., 2018. Transcriptome analysis using RNA-Seq revealed the effects of nitrogen form on major secondary metabolite biosynthesis in tea (*Camellia sinensis*) plants. Acta Physiol. Plant. 40, 127.
Young, M.D., Wakefield, M.J., Smyth, G.K., Oshlack, A., 2010. Gene ontology analysis for RNA-seq: accounting for selection bias. Genome Biol. 11, R14.
Yue, L., Chen, F., Yu, K., Xiao, Z., Yu, X., Wang, Z., Xing, B., 2019. Early development of apoplastic barriers and molecular mechanisms in juvenile maize roots in response to La_2O_3 nanoparticles. Sci. Total Environ. 653, 675–683.
Yue, L., Ma, C., Zhan, X., White, J.C., Xing, B., 2017. Molecular mechanisms of maize seedling response to La_2O_3 NP exposure: water uptake, aquaporin gene expression and signal transduction. Environ. Sci. -Nano 4, 843–855.
Yue, L., Zhao, J., Yu, X., Lv, K., Wang, Z., Xing, B., 2018. Interaction of CuO nanoparticles with duckweed (*Lemna minor. L*): Uptake, distribution and ROS production sites. Environ. Pollut. 243, 543–552.
Yu, X., Choi, S.R., Chhapekar, S.S., Lu, L., Ma, Y., Lee, J.Y., Hong, S., Kim, Y.Y., Oh, S.H., Lim, Y.P., 2019. Genetic and physiological analyses of root cracking in radish (*Raphanus sativus* L.). Theor. Appl. Genet. 132, 3425–3437.
Yu, R., Xu, L., Zhang, W., Wang, Y., Luo, X., Wang, R., Zhu, X., Xie, Y., Karanja, B., Liu, L., 2016. De novo taproot transcriptome sequencing and analysis of major genes involved in sucrose metabolism in radish (*Raphanus sativus* L.). Front. Plant Sci. 7, 585.
Zhang, W., Musante, C., White, J.C., Schwab, P., Wang, Q., Ebbs, S.D., Ma, X., 2017a. Bioavailability of cerium oxide nanoparticles to *Raphanus sativus L.* in two soils. Plant Physiol. Biochem. 110, 185–193.
Zhang, Y., Wang, J., Gong, S., Xu, D., Sui, J., 2017b. Nitrogen fertigation effect on photosynthesis, grain yield and water use efficiency of winter wheat. Agr. Water Manag. 179, 277–287.
Zuverza-Mena, N., Armendariz, R., Peralta-Videa, J.R., Gardea-Torresdey, J.L., 2016. Effects of silver nanoparticles on radish sprouts: root growth reduction and modifications in the nutritional value. Front. Plant Sci. 7, 90.